ELSEVIER

Ceramics International 25 (1999) 69–75

CERAMICS INTERNATIONAL

Effect of NiO addition on the sintering and grain growth behaviour of $BaTiO_3$

W.H. Tzing, W.H. Tuan*

Institute of Materials Science and Engineering, National Taiwan University, Taipei, Taiwan 10764

Received 24 November 1997; accepted 16 January 1998

Abstract

The sintering and grain growth behaviour of NiO-doped $BaTiO_3$ in air are investigated in the present study. The solubility of NiO in $BaTiO_3$ is determined by measuring the lattice constant of $BaTiO_3$ as a function of NiO content. The solubility is around 0.13 wt% as sintering temperature ranges from 1250 to 1330°C. The densification of $BaTiO_3$ is retarded due to the solution of NiO. Possible mechanism is proposed. The existence of residual NiO inclusions also reduces the densification rate. The adding of NiO inhibits the grain growth of $BaTiO_3$. For the $BaTiO_3$ doped with 0.13 wt% NiO, no abnormal grains are observed. © 1998 Elsevier Science Limited and Techna S.r.l. All rights reserved

Keywords: A. sintering; A. grain growth; D. $BaTiO_3$

1. Introduction

Barium titanate ($BaTiO_3$) is widely used as a dielectric material for its high dielectric constant. Due to the capacitance is increased with increasing area, multilayer structure $BaTiO_3$ is developed to fulfil the requirement on size reduction. The material frequently used as the inner electrode for the multilayer capacitors is Pd/Ag alloys. Due to the cost of Pd is high, nickel is considered as an alternative [1]. The nickel may be oxidised during binder pyrolysis in air. Nickel oxide then tends to diffuse into $BaTiO_3$ to change its dielectric properties [2]. The capacitance is also increased with decreasing thickness. However, the thickness of the dielectric is reduced, the influence of Ni solutes on the dielectric properties can be more noticeable.

The solubility of NiO in the $BaTiO_3$ lattice is reported as 0.6 to 1.0 wt% [3–5]. The valence state of Ni ions in BaTiO3 lattice is proved as Ni^{2+} [4,6]. The Ni ions may occupy the Ba^{2+} sites [5,7] or Ti^{4+} sites [3,6]. The dominated sintering mechanism for $BaTiO_3$ is reported as grain boundary diffusion [8,9]. The rate control species for diffusion as proposed by Lewis et al. is Ti ion vacancy [10]. Polycrystalline $BaTiO_3$ readily experiences abnormal grain growth during sintering. Considerable studies have focused on the grain growth behaviour of $BaTiO_3$. The addition of Dy_2O_3, [11] Nb_2O_5 [12] or Sc_2O_3 [13] inhibits the grain growth of $BaTiO_3$. The presence of NiO can also reduce the size of $BaTiO_3$ grains [14].

To the knowledge of the present authors, the effect of NiO on the sintering behaviour of $BaTiO_3$ has not been determined. In the present study, the nickel oxide particles are mixed intimately with $BaTiO_3$ powder before sintering. The solubility of NiO in $BaTiO_3$ is determined first. The effect of Ni solutes or undissolved NiO inclusions, on the sintering behaviour of $BaTiO_3$ can then be determined.

2. Experimental procedures

The $BaTiO_3$ powder (no. 219-6, Ferro Co., USA) having a Ba/Ti ratio of 0.995 was mixed with various amounts of nickel nitrate (Johnson Matthey Chem. Co., USA). The powder mixtures were milled together in ethyl alcohol for 4 h. The grinding media used was zirconia balls. The slurry was dried using a rotary evaporator. The dried lumps were crushed and passed through a plastic sieve. The sieved powder was calcined at 500°C in air for 1 h. The temperature was higher than the decomposition temperature of nickel nitrate. The calcined powder was then formed by uniaxially pressing at 25 MPa into disks (10 mm in diameter and about

* Corresponding author.

0272-8842/98/$—see front matter ©1998 Elsevier Science Limited and Techna S.r.l. All rights reserved
PII: S0272-8842(98)00003-0

5 mm in thickness). The green density of specimens was measured by the geometric method. The pore size distribution of green compacts was characterised by mercury porosimetry (Autopore II 9220, Micromeritics Instrument Co., USA).

Sintering was performed at a temperature varied from 1250–1370°C in air. The dwelling time was 2 h. The heating and cooling rates were 3°C min^{-1}. Shrinkage kinetics was determined by a differential dilatometer (Theta Co., USA). Phase identification was performed by X-ray diffractometry (XRD). A very slow scanning rate (0.01 degree 2θ /s) was also used to determine the lattice constant ratio of c over a by using the (002) and (200) reflections. The size of NiO crystals in the calcined powder was determined by measuring the line broadening of the NiO XRD peaks. The fired density was determined by the water displacement method. The polished specimens were prepared by grinding with SiC particles and by polishing with Al_2O_3 particles. The polished surfaces were chemically etched with a HCl–HF solution to reveal the grain boundaries. The microstructure was observed with scanning electron microscopy (SEM). The volume fraction of abnormal grains was determined by measuring the area fraction of abnormal grains in SEM micrographs. The size of $BaTiO_3$ and NiO grains was determined by using the linear intercept technique. Samples for transmission electron microscopy (TEM, Jeol 10OCXII) were mechanically thinned to about 50 μm. The thinned samples were subsequently dimpled to a thickness of 20 μm in the centre and then ion-milled to perforation of the central disk region. These samples were observed at the voltage of 100 kV.

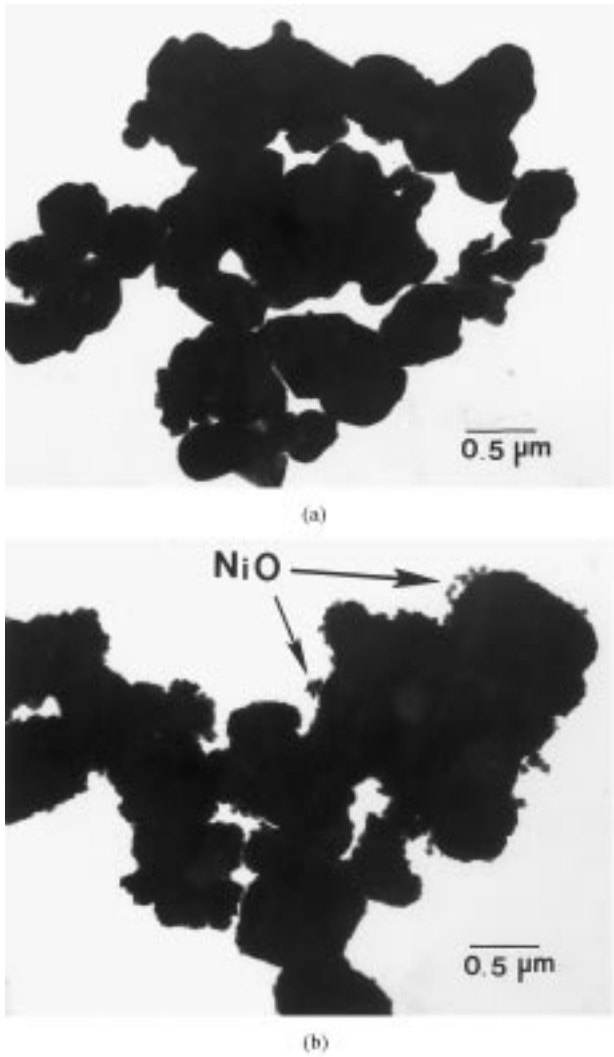

Fig. 1. The morphology of the calcined powders which contain (a) 0 and (b) 12.4 wt% NiO.

3. Results and discussion

There are only tetragonal $BaTiO_3$ and cubic NiO detected in the calcined powder by the XRD analysis. The morphology of the calcined powder is shown in Fig. 1. On the surface of the $BaTiO_3$ particles, small rectangular NiO particles are observed, Fig. 1(b). The size of NiO crystals as determined by the XRD line broadening technique is around 30 nm. The pore size distribution of green bodies is shown in Fig. 2 Bimodal pore size distribution is noted in all green compacts. It suggests that the powder is strongly agglomerated [15]. The strong agglomerates are survived after the die-pressing stage. The mean pore size within the agglomerates (intra-agglomerate) is about 0.18 μm. The amount of intra-agglomerate pores is little. Most pores are located at inter-agglomerate sites. The size of inter-agglomerate pores for pure $BaTiO_3$ is 0.26 μm. As 0.13 wt% NiO is added, the size of inter-agglomerate pores is virtually unchanged. However, as NiO content is higher than 1.3 wt%, the size of inter-agglomerate pores increases with increasing NiO content. The surface of $BaTiO_3$ particles is coated with small NiO particles. The presence of small NiO particles can push the $BaTiO_3$ particles further apart. The size of inter-agglomerate pore is thus increased.

The green density is shown as a function of NiO content in Fig. 3. As the NiO content is below 1.3 wt%, the green density is around 53%. As the NiO content is higher than 1.3 wt%, the green density is decreased due to the size of pores is enlarged, Fig. 2. The XRD patterns of the sintered specimens are shown in Fig. 4. Only tetragonal $BaTiO_3$ phase and cubic NiO phase are detected as sintering temperature is below 1330°C (Fig. 4(a)). There is no NiO detected in the $BaTiO_3$–1.3 wt% NiO specimen. However, due to the detection limit of the XRD analysis, the XRD analysis can only suggest that the solubility of NiO in $BaTiO_3$ is below 1.3 wt%. A monoclinic phase, $Ba_6Ti_{17}O_{40}$ phase, is found as the sintering temperature is 1370°C (Fig. 4(b)).

The presence of the $Ba_6Ti_{17}O_{40}$ phase suggests the presence of an eutectic liquid during sintering.

Fig. 5 shows typical XRD patterns obtained by using the slow scanning rate. The splitting of (002) and (200) reflections of tetragonal phase decreases with increasing NiO content. The lattice constant ratio of c over a of $BaTiO_3$ is shown as a function of NiO content in Fig. 6 Two factors affect the c/a ratio. The factors are the grain size and the solution of NiO in $BaTiO_3$. Alrt reported that c/a ratio is reduced with decreasing grain size as the grain size is smaller than 1 μm [16]. The c/a ratio is constant for the specimens with grain size above 1.5 μm. To be shown latter, the grain size measured for the specimens investigated in the present study is larger than 1.2 μm. The major factor to reduce the c/a ratio is thus the solution of NiO in $BaTiO_3$ lattice. The c/a ratio is decreased as NiO content is increased (Fig. 6). As the NiO content is higher than a certain value, the values of c/a ratio are stabilized. The solubility of NiO in $BaTiO_3$ can thus be determined by using Fig. 6. As the sintering temperature ranges from 1250 to 1330°C, the solubility of NiO in $BaTiO_3$ is about 0.13 wt%. As the sintering temperature is 1370°C, the solubility is higher than 0.13 wt% and lower than 1.3 wt%. It may be due to the presence of the eutectic liquid that enhances the solubility. The solubility limit obtained in the present study is lower than the values reported by others [3–5]. The discrepancy may result from the different raw material used.

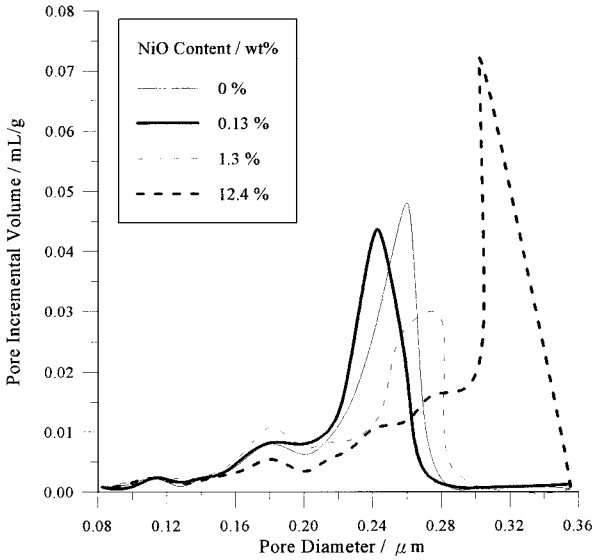

Fig. 2. The pore size distribution for the green bodies containing different NiO content.

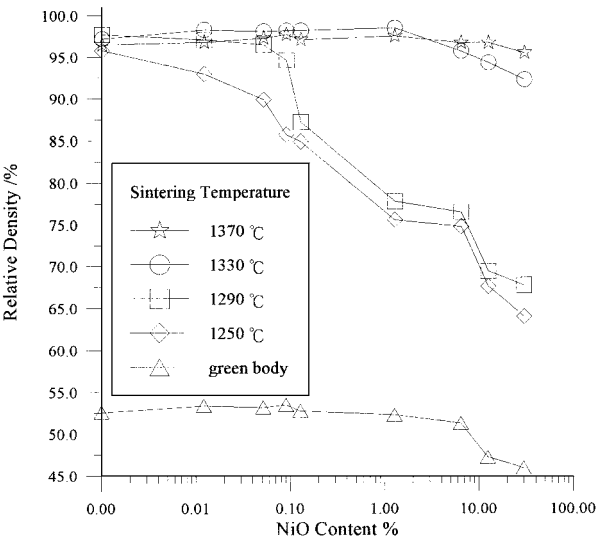

Fig. 3. The relative density of NiO-doped $BaTiO_3$ specimens as a function of NiO content.

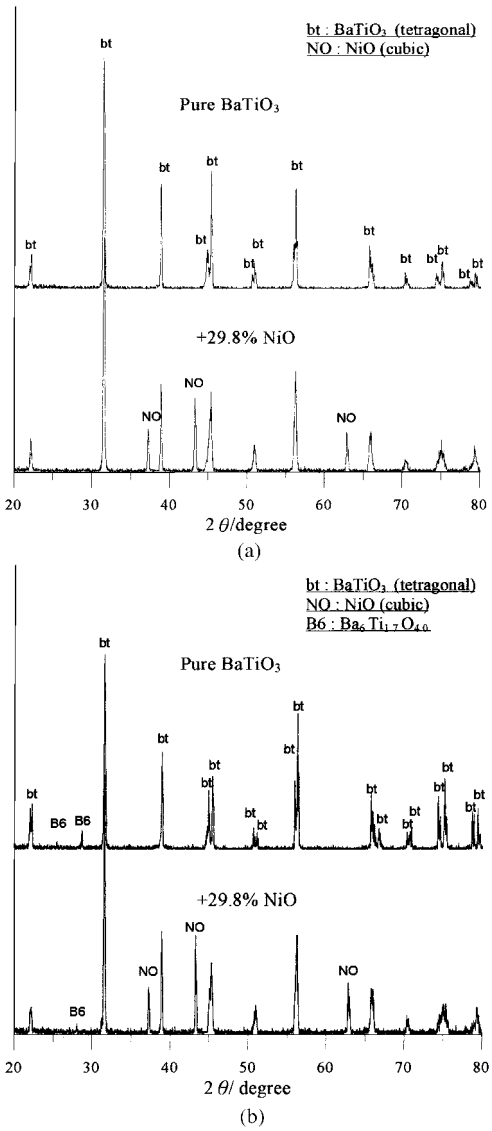

Fig. 4. The XRD patterns of undoped and 29.8 wt% NiO-doped $BaTiO_3$ specimens sintered at (a) 1330°C and (b) 1370°C.

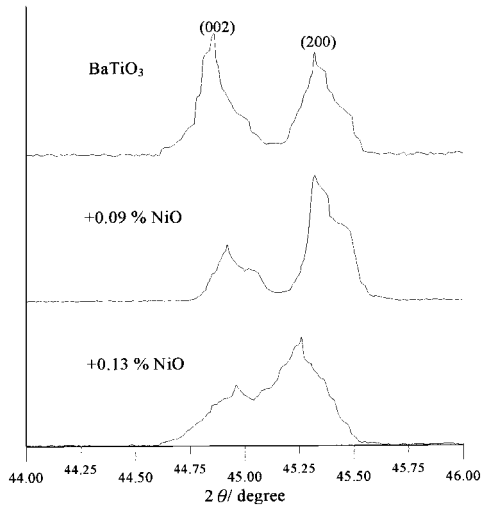

Fig. 5. The (002) and (200) diffraction peaks for NiO-doped $BaTiO_3$ specimens. The specimens are sintered at 1330°C for 2 h.

When the coordination number is 6, the ionic radius of the Ti^{4+} and Ni^{2+} is 0.61 and 0.69Å, respectively. The ionic radius of Ba^{2+} ion is 1.59 Å as the coordination number is 12. Although the valence of Ni ion is the same as that of Ba ion, the ionic radius of Ni^{2+} is much smaller than that of Ba^{2+}. The Ni^{2+} is more likely to replace the Ti^{4+} for their similar ionic size. This has been proved recently [17]. Tzing and Tuan found that *n*-type semiconducting $BaTiO_3$ is obtained as sintering is taken place in a reducing atmosphere. The presence of Ni ion increased the electrical resistivity. It suggested that Ni ion acts as electron acceptor in $BaTiO_3$ lattice. The replacement of Ti^{4+} by Ni^{2+} may accompany the formation of oxygen vacancy as [6]

$$NiO \xrightarrow{BaTiO_3} Ni_{Ti}'' + V_o^{\bullet\bullet} + O_o \quad (1)$$

The $BaTiO_3$ crystal is distorted due to the solution of Ni. The fraction of the increase in *a*-axis is higher than that in *c*-axis. The *c*/*a* ratio is thus reduced. The low solubility may result from different valence state between Ti^{4+} and Ni^{2+}.

The relative density of sintered specimens is also shown in Fig. 3. The relative density of the undoped $BaTiO_3$ is higher than 95%. As NiO is added, the relative density is decreased with the increase of NiO content as sintering temperature is below 1290°C. It indicates that the addition of NiO retards the densification of $BaTiO_3$. The shrinkage is isotropic for all the specimens prepared in the present study. The relative density during sintering can thus be calculated by using the linear shrinkage data from dilatometer. The densification kinetics for the NiO-doped $BaTiO_3$ are shown in Fig. 7. A constant heating rate, 3°C min^{-1} is used during sintering in the dilatometer. The densification rate can be estimated by differentiating the relative density with temperature (Fig. 8). Two peaks are found in the densification rate curves. There is a similarity between the densification rate and the pore size distribution curves, (Figs. 2 and 8). It implies that the first peak in the densification rate curves is resulted from the shrinkage of the small intra-agglomerate pores. The second peak is resulted from the shrinkage of the inter-agglomerate pores.

The densification is mainly started roughly from 1150°C (Fig. 8). It is interesting to examine whether the solution of NiO in $BaTiO_3$ or the densification takes place first. A 0.13 wt% NiO-doped $BaTiO_3$ is sintered at 1100°C for 1 min. The *c*/*a* ratio for the doped specimen is 1.0095 which is less than the value for the undoped $BaTiO_3$. It thus indicates that NiO starts to dissolve into $BaTiO_3$ before 1100°C. The solution of NiO in $BaTiO_3$ takes place before the densification. When the added

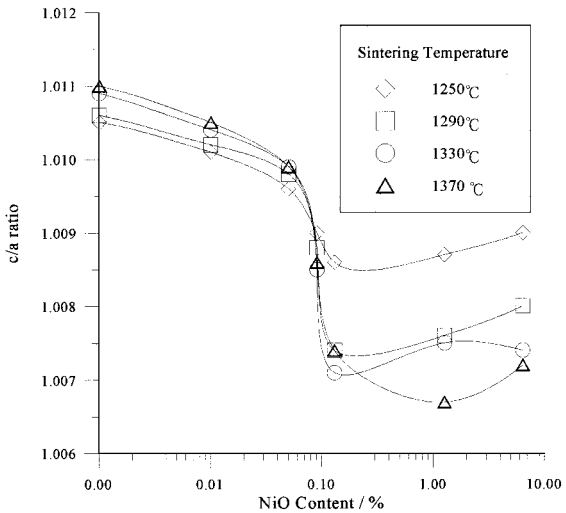

Fig. 6. The lattice constant *c*/*a* ratio of NiO-doped $BaTiO_3$ specimens as a function of NiO content.

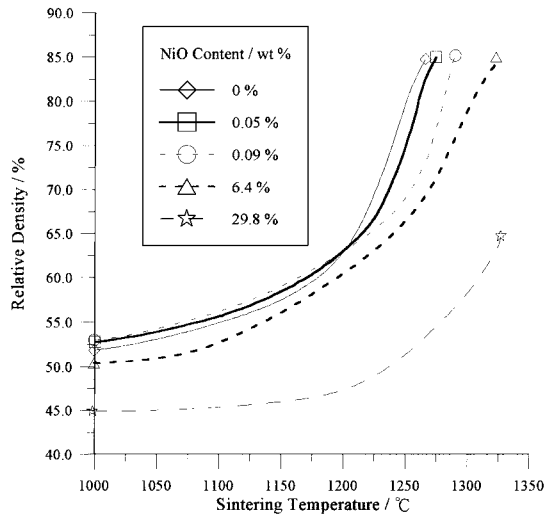

Fig. 7. The densification curves for NiO-doped $BaTiO_3$ specimens as a function of temperature.

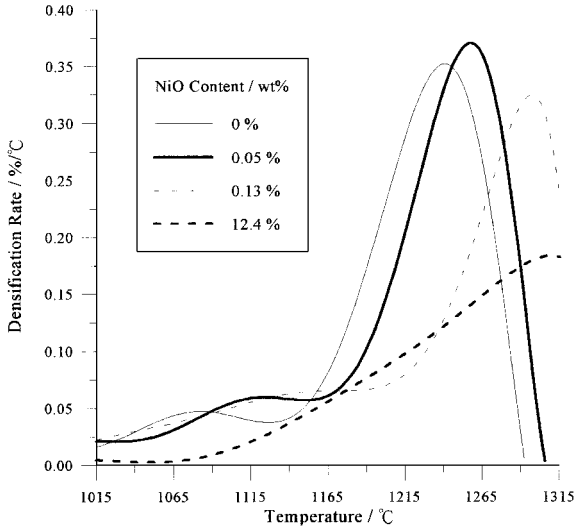

Fig. 8. The densification rate of NiO-doped $BaTiO_3$ specimens as a function of temperature.

NiO content is below the solubility limit, higher temperature is needed to reach maximum densification rate. It indicates the densification of $BaTiO_3$ is retarded due to the presence of Ni solute. The solution of NiO into $BaTiO_3$ increases the concentration of $V_o^{\cdot\cdot}$ Eq. (1). As Schottky-type, defect is predominant in $BaTiO_3$ [18], the increase of the concentration of $V_o^{\cdot\cdot}$ reduces the concentration of V_{Ti}''''. The Ti vacancy is the rate controlling species because it has the highest activation energy of diffusion in $BaTiO_3$ [10]. The solution of NiO thus retards the densification of $BaTiO_3$.

As the NiO content is higher than the solubility limit, residual NiO inclusions can be observed, (Fig. 9). The presence of NiO inclusions between $BaTiO_3$ grains increases the inter-diffusion distance. The densification rate and final density are thus reduced (Figs. 3 and 8).

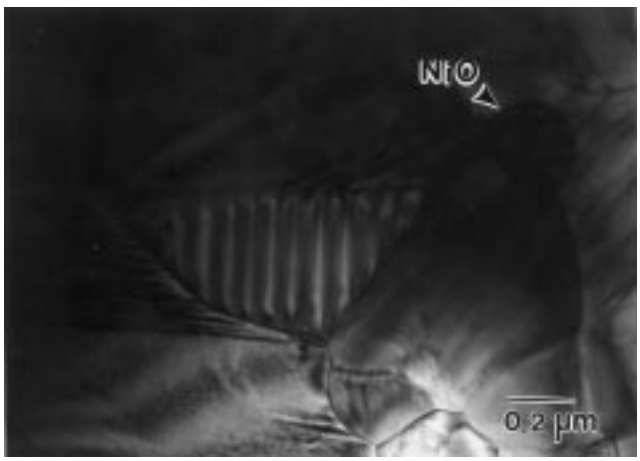

Fig. 9. A TEM micrograph of the 1.3 wt% NiO-doped $BaTiO_3$ specimen. The specimen is sintered at 1330°C.

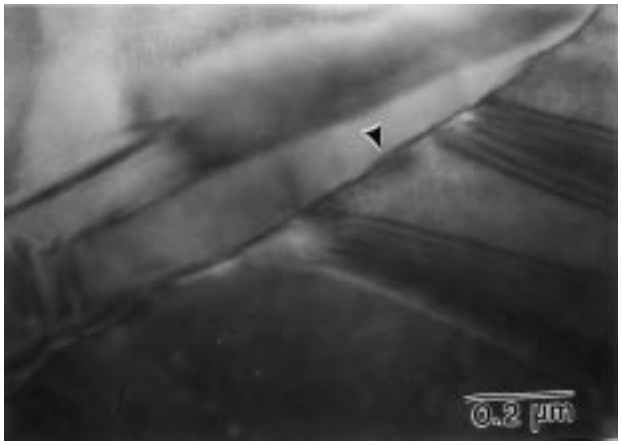

Fig. 10. The liquid phase observed in the undoped $BaTiO_3$ specimen sintered at 1330°C.

According to the $BaO–TiO_2$ phase diagram [19], an eutectic liquid phase is formed above 1312°C in the TiO_2 excess system. The liquid phase is observed in the specimens sintered at 1330°C (Fig. 10). The presence of the liquid phase also enhances the densification of NiO-doped $BaTiO_3$ specimens (Fig. 3). As the sintering temperature is 1370°C, the relative density of the 30 wt% NiO-doped $BaTiO_3$ is higher than 95%.

Typical microstructures of pure $BaTiO_3$ and NiO-doped $BaTiO_3$ are Shown in Fig. 11. The size of abnormal and small grains is shown in Fig. 12. The volume fraction of abnormal grain is shown in the bracket in the figure. Abnormal grains can be observed in the $BaTiO_3$ specimen sintered at 1250°C. This temperature is lower than the $BaTiO_3–Ba_6Ti_{17}O_{40}$ eutectic temperature [19]. As shown in Fig. 2, agglomerates are presented in the green compacts. The shrinkage of the intra-agglomerate pores takes place in the very beginning of the sintering (Fig. 8). The abnormal grains may nucleate from the dense agglomerates. Chemical inhomogeneity can reduce the liquid formation temperature. The possible formation of liquid phase may also play some role on the formation of abnormal grains. The volume fraction of abnormal grains, the size of abnormal and of small grains increase with increasing sintering temperature. The size of $BaTiO_3$ grains in the undoped $BaTiO_3$ specimens grow to a size of 50 μm as they are sintered above 1330°C, (Fig. 11(b)). Many pores are trapped in the abnormal grains. It leads to the decrease of relative density.

The microstructure of a NiO-doped $BaTiO_3$ sintered at 1330°C is shown in Fig. 11(c). The added NiO content is 0.13 wt%. The relative density is about 98.2%. No abnormal grains are observed due to the existence of some NiO inclusions. The size of NiO inclusions in all the NiO-doped $BaTiO_3$ is smaller than 0.7 μm. When NiO content is below the solubility limit, the inhibition of grain growth can be attributed to the retardation of

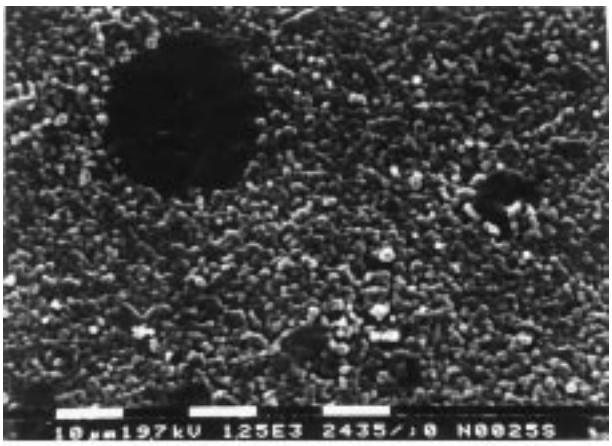

(a)

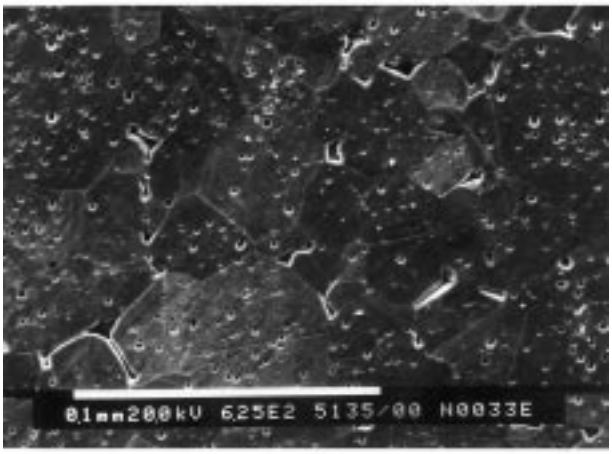

(b)

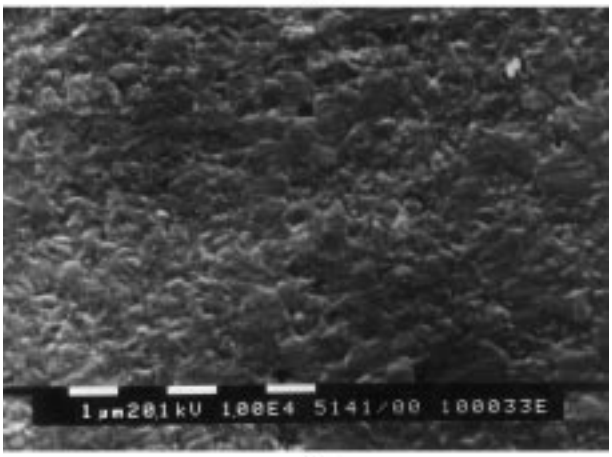

(c)

Fig. 11. The SEM micrographs of (a) $BaTiO_3$ sintered at 1250°C, (b) $BaTiO_3$ sintered at 1330°C and (c) 0.13 wt% NiO-doped $BaTiO_3$ sintered at 1330°C.

densification [20]. When NiO content is higher than the solubility limit, the presence of NiO inclusions prohibits the movement of grain boundaries (Fig. 9). The microstructure of these specimens is refined despite the presence of liquid phase.

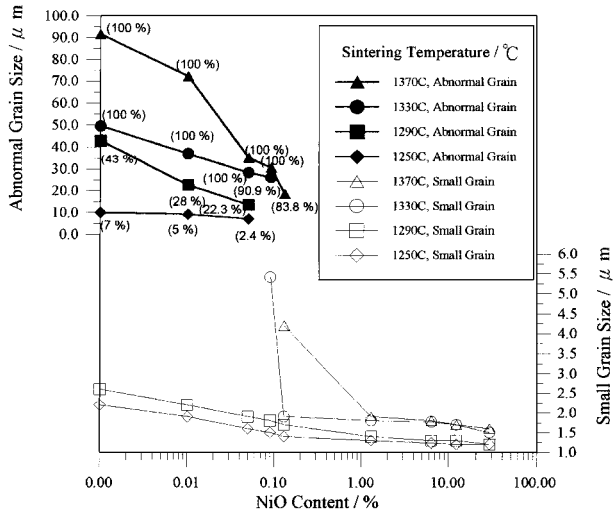

Fig. 12. The average size of $BaTiO_3$ grains in the NiO-doped. $BaTiO_3$ specimens. The number in the bracket indicates the volume fraction of abnormal $BaTiO_3$ grains.

4. Conclusions

The following conclusions can be made from the present study:

1. Around 0.13 wt% NiO is dissolved into $BaTiO_3$ as the sintering temperature varies from 1250 to 1330°C. The presence of the eutectic liquid increases the solubility.
2. When the added NiO content is below the solubility limit, higher temperature is needed to reach maximum densification rate. The densification of $BaTiO_3$ is retarded due to the presence of Ni solute.
3. The presence of residual NiO inclusions reduces the sintered density. Raising the sintering temperature to form an eutectic liquid enhances the sinterability.
4. Both the Ni solute and NiO inclusions reduce the grain size of $BaTiO_3$. The abnormal grains are totally suppressed as the NiO content is higher than the solubility limit.

Acknowledgements

The comments given by Dr. Simmon H-P. Li, National Taiwan University, were very helpful.

References

[1] Y. Sakabe, Dielectric materials for base-metal multilayer ceramic capacitors, Am. Ceram. Soc. Bull. 66 (1987) 1338–1341.
[2] M. Kahn, D.P. Burks, W. Schulze, Ceramic capacitor technology, in: L.M. Levison (Ed.), Electronic Ceramics–Properties,

Devices and Application, Marcel Dekker, New York, 1988, pp. 191–274.
[3] H. Emoto, J. Hojo, Sintering and dielectric properties of $BaTiO_3$–Ni composite ceramics, J. of Ceram. Soc. of Japan, Int. Ed. 100 (1992) 553–557.
[4] H. Ihrig, The phase stability of $BaTiO_3$ as a function of doped 3d elements: an experimental study, J. Phys. C: Solid State Phys. 11 (1978) 819–287.
[5] P. Baxter, N.J. Hellicar, B. Lewis, Effect of additives of limited solid solubility on ferroelectric properties of barium titanate ceramics, J. Am. Ceram. Soc. 42 (1959) 465–470.
[6] H.-J. Hagemann, D. Hennings, Reversible weight change of acceptor-doped $BaTiO_3$, J. Am. Ceram. Soc. 64 (1981) 590–594.
[7] W.W. Coffeen, Dielectric bodies in metal stannate–barium titanate binary systems, J. Am. Ceram. Soc. 37 (1954) 480–489.
[8] Y. Enomoto, A. Yamaji, Preparation of uniformly small-grained $BaTiO_3$, Am. Ceram. Soc. Bull. 60 (1981) 566–750.
[9] L.A. Xue, Y. Chen, E. Gilbart, R.J. Brook, The kinetics of hot-pressing for undoped and donor-doped $BaTiO_3$ ceramics, J. Mater. Sci. 25 (1990) 1423–1428.
[10] G.V. Lewis, C.R.A. Catlow, R.E.W. Casselton, PTCR effect in $BaTiO_3$, J. Am. Ceram. Soc. 68 (1985) 555–558.
[11] A. Yamaji, Y. Enomoto, K. Kinoshita, T. Murakami, Preparation, characterization, and properties of Dy-doped small-grained $BaTiO_3$ ceramics, J. Am. Ceram. Soc. 60 (1977) 97–101.
[12] M. Kahn, Preparation of small-grained and large-grained ceramics from Nb-doped $BaTiO_3$, J. Am. Ceram. Soc. 54 (1971) 452–454.
[13] K.S. Mazdiyasni, L.M. Brown, Microstructure and electrical properties of SC_2O_3-doped, rare-earth-oxide-doped, and undoped $BaTiO_3$, J. Am. Ceram. Soc. 54 (1971) 539–543.
[14] H. Ihrig, PTC effect in $BaTiO_3$ as a function of doping with 3d elements, J. Am. Ceram. Soc. 64 (1981) 617–620.
[15] C.H. Lu, W.H. Tuan, B.K. Fang, Effects of pre-sintering heat treatment on the microstructure of barium titanate, J. Mater. Sci. Letters 15 (1996) 43–45.
[16] G. Arlt, D. Hennings, G. de With, Dielectric properties of fine-grained barium titanate ceramics, J. Appl. Phys. 58 (1985) 1619–1625.
[17] W.H. Tzing, W.H. Tuan, Dielectric properties of NiO-doped $BaTiO_3$ sintered with different oxygen partial pressure. Euro Ceramics V, part 2, Paris, 1997, pp. 1167–1170.
[18] J. Nowotny, M. Rekas, Defect structure, electrical properties and transport in barium titanate. VI. General defect model, Ceram. Int. 20 (1994) 257–263.
[19] H.M. O'Bryan, L. Thomson, Phase equilibria in the TiO_2-rich region of the system BaO–TiO_2, J. Am. Ceram. Soc. 57 (1974) 522–526.
[20] H.L. Hsieh, T.T. Fang, Effect of green states on sintering behavior and microstructure evolution of high-purity barium titanate, J. Am. Ceram. Soc. 73 (1990) 1566–1573.